Heliyon

ELSEVIER

Received:
3 November 2018
Revised:
21 January 2019
Accepted:
8 April 2019

Cite as:
Sathish-Kumar Kamaraj, Alejandro Esqueda Rivera, Selvasankar Murugesan, Jaime García-Mena, Otoniel Maya, Claudio Frausto-Reyes, José Tapia-Ramírez, Hector Silos Espino, Felipe Caballero-Briones. Electricity generation from Nopal biogas effluent using a surface modified clay cup (*cantarito*) microbial fuel cell. Heliyon 5 (2019) e01506.
doi: 10.1016/j.heliyon.2019.e01506

Electricity generation from Nopal biogas effluent using a surface modified clay cup (*cantarito*) microbial fuel cell

Sathish-Kumar Kamaraj [a,*], Alejandro Esqueda Rivera [b], Selvasankar Murugesan [c], Jaime García-Mena [c], Otoniel Maya [c], Claudio Frausto-Reyes [d], José Tapia-Ramírez [c], Hector Silos Espino [a], Felipe Caballero-Briones [e]

[a] *Laboratorio de medio ambiente sostenible y Laboratorio de Cultivo de Tejidos Vegetales, Instituto Tecnológico El Llano (ITEL)/ Tecnológico Nacional de México (TecNM), Aguascalientes. Km 18 carr, Aguascalientes-San Luis Potosí, El Llano Ags., C.P. 20330, Mexico*

[b] *Universidad Politécnica de Aguascalientes, Ingeniería en Energía, Calle Paseo San Gerardo No. 207, Fracc. San Gerardo, Aguascalientes, Ags., 20342, Mexico*

[c] *Departamento de Genética y Biología Molecular, Cinvestav-IPN, México DF, D.F. 07360, Mexico*

[d] *Centro de Investigaciones en Óptica, A.C., Unidad Aguascalientes, Prol. Constitución 607, Fracc. Reserva Loma Bonita Aguascalientes, 20200, Mexico*

[e] *Instituto Politécnico Nacional, Materials and Technologies for Energy, Health and Environment (GESMAT), CICATA Altamira, Km 14.5 Carretera Tampico-Puerto Industrial Altamira, 89600, Altamira, Mexico*

[*] Corresponding author.
E-mail addresses: sathish.bot@gmail.com, sathish.k@llano.tecnm.mx (S.-K. Kamaraj).

Abstract

A modified clay cup (cantarito) microbial fuel cell (C-MFCs) was designed to digest the biomass effluent from a nopal biogas (NBE). To improve the process, commercial acrylic varnish (AV) was applied to the C-MFCs. The experiment was performed as:Both-C-MFCs, painting of AV on both sides of the clay cup; In-C-MFCs, painting of AV on the internal side, and Out-C-MFCs painting of AV on the external side. The order for the maximum volumetric power densities were Both-C-MFCs (1841.99 mW/m^3)>Out-C-MFCs (1023.74 mW/m^3) >In-C-MFCs (448.90 mW/m^3). The control experiment without applied varnish did not show a stable potential, supporting the idea that the acryloyl group in varnish

https://doi.org/10.1016/j.heliyon.2019.e01506

could favor the performance. Finally, a 4-digits clock was powered with two, Both-C-MFCs connected in series; the microbial diversity in this format was explored and a well-defined bacterial community including members of the phyla Actinobacteria, Bacteroidetes, Firmicutes, Proteobacteria, Synergistetes and candidate division TM7 was found.

Keyword: Energy

1. Introduction

In recent days, the bio-based economy has been attaining the significant attraction in the energy sector. The emerging concept of the biorefinery is produced multiple fuels and value-added by-products such as bioethanol, biodiesel, biogas and chemicals, materials, food, and feed from biomass feedstock. The ability to convert the biofuels from the biomass results in waste streams, amenable to further energy recovery with the support of microbial fuel cells (Cherubini, 2010; ElMekawy et al., 2013). The potential of Microbial fuel cells (MFCs) has the ability to direct conversion of electrical energy from the organic materials, where biocatalyst plays a vital part. The implementation of MFCs system in biorefinery process has the dual advantages that extracted energy recovery from the discarded biomass after either completion of fuels or value-added by-product production and reduce the waste streams (Borole et al., 2013; Ucar et al., 2017). Complex organic electron donor at the anodic chamber not alone influences on microbial community, also influence the power production and economic viability (Zhi et al., 2014; Zhao et al., 2017). Diverge organic substrate such as low molecular sugar to a complex organic material containing carbohydrates, proteins, volatile acids and wastewater were exploited to generate the electricity in MFCs (Zhang et al., 2011; Chae et al., 2009; Pant et al., 2010). The bio-electrochemical systems have the potential substrate conversion into products or fuels depends on the chemical composition and the concentration of organic substrates (Kondaveeti et al., 2014). There has been limited information on the deployment of complex waste/spend biomass feedstock into direct electricity generation through MFCs. Consequently, our research interest was focused on spending biomass effluent from Nopal biogas plant in Calvillo, Ags., Mexico, in order to improve resource utilization, reduction of the waste stream and further energy production through MFCs system.

The function of separators is one of the noteworthy factors influence the MFCs power generation which physically separates the anodic and cathodic chamber. As it could conjure up for the protons transfer to the cathode and prevent the permeable of oxygen to the anode (Min et al., 2005). Inferentially the separator could possess the negative charge on the backbone ($-PO_3^-$,$-COO^-$, $-C_6H_4O^-$ and SO_3^-) subsequently, it facilitates the cations crossover them (Hideo et al., 1991). There are

https://doi.org/10.1016/j.heliyon.2019.e01506

different kinds of separators which were used in MFC, such as Ultrex, Nafion, bipolar membranes, dialyzed membrane, polystyrene and divinylbenzene with the sulfuric acid group, glass wool, nano-porous filters and micro filtration membranes (Rahimnejad et al., 2012). Among these, Nafion is one of the most common separators in MFCs. However, the utilization of Nafion in the wastewater provokes the unspecific transport of other cations (Rozendal et al., 2006).

Additionally, the high cost and oxygen permeability of Nation (Doyle and Rajendran, 2010) limits its usage in MFCs. For the above-mentioned fact, the researcher had an interest in searching for alternative ceramic-based materials. In this way, There was a successful implementation of different ceramic-based materials on MFCs (Ajayi and Weigele, 2012; Winfield et al., 2013). Earthenware clay based two-chamber MFCs used permanganate as electron acceptor at cathode operated under continuous flow conditions the power density reached 70.48 W/m^3 (Behera and Ghangrekar, 2011).

The comparison of earthenware and terracotta employed on air cathode MFCs showed that the earthenware based MFC generates 75% more power than terracotta based MFCs. Furthermore, the performance of earthenware MFCs had a similar level of performance in cation exchange membrane seed MFCs (Winfield et al., 2013). Thus, ceramic-based MFCs may be a sustainable cost-effective alternative for power production, if a complex organic substrate could be used as an electron donor. Many studies in the literature focus ceramic materials optimum power production by considering the composition of ceramic, thickness and porosity (Ajayi and Weigele, 2012; Winfield et al., 2013). However, there is a lack of information about the surface modification of ceramic separators.

The aim of this work is to exploit the Nopal biogas effluent as a medium to be a treatment anode in the two compartments cost-effective small size clay cup (*cantarito*) modified microbial fuel cells (C-MFCs). Further, the surface of the clay cup altered by acrylic based commercial varnish, in order to achieve the optimal power production on C-MFCs. Additionally, metagenomics studies reveal the diversity of the microbial community at the initial and final stage of MFC operation. Enhanced power production was demonstrated by connecting the two C-MFCs in series to power 4 digital clocks.

2. Material and methods

2.1. Collection of nopal biomass effluent

The Nopal Biomass effluent was made with prickly pear cacti mixed with cattle dunk waste in the proportion of 80:10. Then it was left to decompose, producing methane gas. After that, it was used for fuel and burned to generate enough electricity (Mason

https://doi.org/10.1016/j.heliyon.2019.e01506

et al., 2015). At the final stage, the discharged Nopal biomass effluent was collected from the plant situated in Calvillo, Aguascalientes, Mexico and stored in a refrigerator at 4°Cfor further use.

2.2. Construction of dual chamber cantarito modified microbial fuel cells

A clay cup (*cantarito* -3mm thickness) was procured from the local market of Aguascalientes (Mercado Teren, Aguascalientes, Mexico.). Graphite felt used as an anode and cathodic current collector (Fuel Cell store, U.S.A). The inside of clay cup is filled with the potassium ferricyanide (100 mM) solution (Karthikeyan et al., 2009), and the outside of the clay cup contains the Nopal biomass effluent (150 mL), which was served as inoculum in the anode and also as a medium to be a treat. The whole container was air tighten (Mexican Patent registration number bending). Further, the water-based acrylic commercial varnish was painted as following experiments: inside of clay cup was pained (In-C-MFCs), outside of clay cup (Out-C-MFCs) and Both side of the clay cup (Both-C-MFCs)".

2.3. Characterization of nopal biomass effluent

The COD, pH, TDS, and conductivity of the Nopal biomass effluent (NBE) were determined according to the Standard Methods (APHA, 1998) with the aid of Henna Instruments.

2.4. Electrochemical characterization of C-MFCs

The C-MFCs were characterized by linear sweep voltammetry (LSV) at 0.1 mV s-1 using Gamry Interface 1000 Potentiostat/Galvanostat/ZRA, starting from the measured open circuit potential up to +50 mV (Kamaraj et al., 2015). Impedance spectra of microbial fuel cells were obtained at the open circuit potential (Eocp). The amplitude of the signal perturbation was 10 mV. It was scanned in the frequency range from 100 kHz to 1 mHz. Data fitting was accomplished by Z-view software. In the long-term operation, all the C-MFCs were at 696 hours with 3KOhms. The voltage was measured and recorded with Arduino Mega.

The current intensity (I) was calculated by Ohm's law: $I=E/R$

(1) The delivered power was obtained as the product of the current intensity times the voltage, that is: $P=I \times E$

(2) At the final stage, the Both-C-MFCs with the best performance was selected and connected in series to power the 4 digital clocks operated for 1008 hrs of batch operations.

https://doi.org/10.1016/j.heliyon.2019.e01506

2.5. Physicochemical characterization of clay cub

Clay cup and acrylic varnish painted clay cup were analysed by EDAX Zeiss HRSEM Auriga 3916 microscope equipped with a Schottky field emission GENIMI column, Elemental composition and mapping of the catalyst were measured by an Energy Dispersive X-ray (EDX) detector attached to the microscope. Further, the FT-IR was performed with Thermo Scientific™ Nicolet™ iS™5.

2.6. 16S rDNA libraries preparation for high throughput sequencing

Bacterial Genomic DNA was extracted from 250 μL slurry from C-MFCs using Power soil DNA Isolation Kit (MoBio Laboratories). The quantity and quality of purified DNA were assessed by 260/280 absorbance using a NanoDrop Lite Spectrophotometer (Thermo Scientific); electrophoretic fractionation in 0.5% agarose gels, stained with Midori Green (Cat. MG02, Nippon Genetics); and recorded using BIO-RAD Molecular Imager Gel DOC XR + Imaging System. For the preparation of DNA libraries for C-MFCs, proper amplicons of approximately 281 bp, including the V3 polymorphic region of 16S rDNA, were amplified using previously reported forward and reverse primers (Murugesan et al., 2015). The thermocycler program was 5 min at 95 °C; 25-cycles [15 s, 94 °C; 15 s, 62 °C; 15 s, 72 °C] followed by 10 min at 72 °C. An amplification was carried out using GeneAmp PCR System 2700 Thermocycler (Applied Biosystems).

2.7. Massive DNA semiconductor sequencing

Amplicons were high-throughput sequenced as previously described (Murugesan et al., 2015). In our case, emulsion PCR was carried out using Ion OneTouchTM 400 Template Kit v2 DL (Thermo Fisher Scientific) following the manufacturer's instructions. The sequencing was done using the Ion 318 v2 Chip and the Ion Torrent PGM System. After sequencing, reads were filtered by the PGM software to remove low quality and polyclonal sequences. During this process, sequences matching the 3′-adapter were automatically trimmed and filtered. Sequence data from this study are part of the Sequence Read Archive (SRA) DDBJ/EMBL/GenBank, under accession number PRJNA352563.

2.8. Analysis of sequenced data for microbial diversity

Sequencing data were analyzed using Ion Torrent PGM software, Torrent Suite v4.0.2 as previously reported (García-Mena et al., 2016). Demultiplexed sequencing data was analyzed using QIIME v.1.9.0 pipeline (Caporaso et al., 2010). Closed reference operational taxonomic units (OTUs) were determined at the 97.0 % similarity level using the UCLUST algorithm. Chimeras were detected and removed

https://doi.org/10.1016/j.heliyon.2019.e01506

from the datasets using the Chimera Slayer. Sequence alignments were done against the Green genes core set (DeSantis et al., 2006).

2.9. Prediction of functional profiling of microbial communities

Functional Profiling of predictive C-MFCs was analyzed by using PICRUSt [Langille et al.,2013 34]. This was done by picking OTUs against the Greengenes database. The output file was further analyzed using Statistical Analysis of Metagenomic Profiles (STAMP) software package (Parks et al., 2014).

3. Results and discussion

3.1. Electrochemical characterization of C-MFCs

Nopal biomass effluent (NBE) was introduced into the anodic chamber, where this could be served as effluent to be treated as inoculum. The open circuit potential of C-MFCs. The maximum open circuit potentials (OCP)of the C-MFCs as follows the order: In-C-MFCs (Max OCP of 1.3587 V at 152.66 hrs and stable period of 7.5 hrs) >Out-CMFCs (Max OCP of 1.0753 V at 99.83 hrs of stable period of 15 hrs) > Both-C-MFCs (Max OCP of 0.9238 V at 165.91 hrs and stable period of 27.75 hrs) >Not-C-MFCs (Max OCP of 0.1857 V at 1.2 hrs and stable period of 3.5 hrs) (Fig. 1). When analyzing the performance of the side painted with acrylic varnish on C-MFCs, In-C-MFCs has discovered that it had a very short period of stability and later it continued to decrease, however, In-C-MFCs exhibited the max OCP. It can be inferred that the protons liberate from the complex substrate at the anode typically shows the lesser concentration than other cations (Rozendal et al., 2006), further those protons might diffuse along with other cations on the

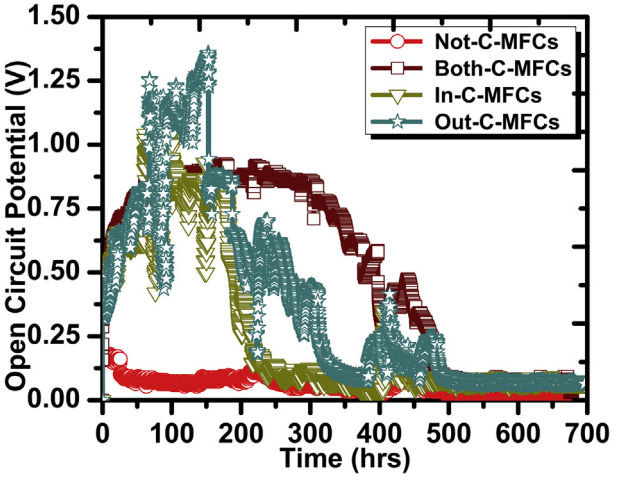

Fig. 1. Open circuit potential of In-C-MFCs (Triangle), Out-C-MFCs (Star), Both-C-MFCs (Cube) and Not-C-MFCs (Circular).

https://doi.org/10.1016/j.heliyon.2019.e01506

clay surface and reach the cathode. The saturation of various cations at the cathodic border could result in a shorter decline of OCP. Whereas Out-C-MFCs doubled the period of stability. Moreover, in Out-C-MFCs, acrylic varnish on the outside of clay cup would resist the unspecific cations enters to clay and conduct proton towards the cathode, which improved the stability for an extended period of OCP. This effect was extended by applying varnish on both sides, and shown in the developed superior stability in comparison with all the other C-MFCs. Unexpectedly, Not-C-MFCs show the least OCP with the lesser period of time. This could be associated with the crossing over complications (Winfield et al., 2013). That experiment gives an indication that the application of acrylic based varnish on the surface of the clay would improve the stability of open circuit potential.

Through the open circuit potential operation of C-MFCs, we also performed the intermittent (every 96 h) electrochemical characterization (linear sweep voltammetry, and EIS) of C-MFCs. From the polarization curve, the maximum volumetric power densities were the following: Both-C-MFCs (1841.99 mW/m^3) >Out-C-MFCs (1023.74 mW/m^3) > In-C-MFCs (448.90 mW/m^3)> Not-C-MFCs (81.70 mW/m^3) (Fig. 2). Both C-MFCs gradually achieved a maximum volumetric power density, higher than all other C-MFCs. It shows the highest stable power production in a longer period. This can be explained by the presence of acrylic based varnish on both sides of the clay, which means it could improve the specific proton diffusion, obtaining, as a result, a higher power production. Moreover, the acrylic functional

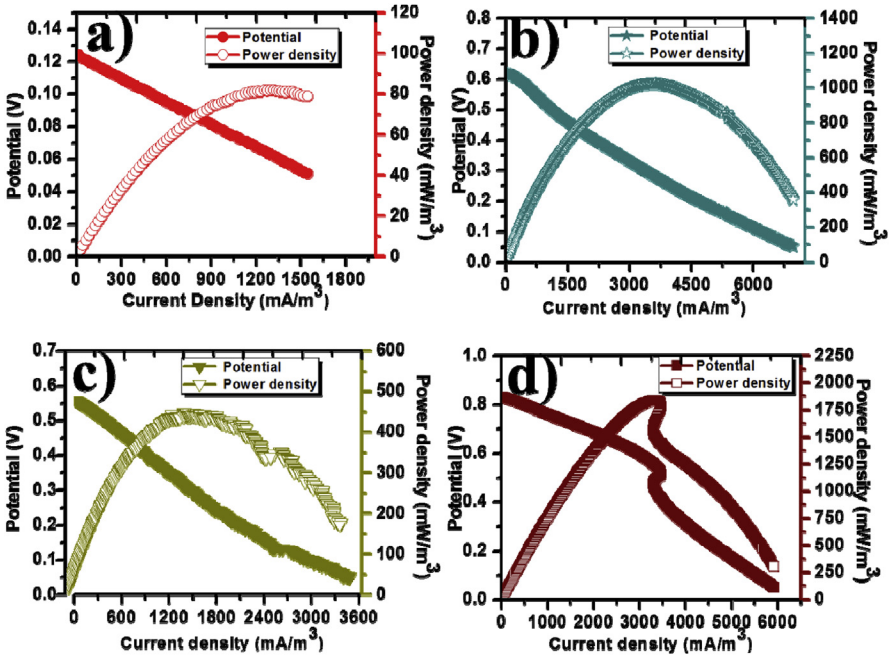

Fig. 2. Polarization curve of In-C-MFCs Not-C-MFCs (Circular-a), Out-C-MFCs (Star-b) (Triangle-c), and Both-C-MFCs (Cube-d).

https://doi.org/10.1016/j.heliyon.2019.e01506

group has been already known for the specific proton conduction (Horan et al., 2009).

Out-C-MFCs reveal the highest power than the In-C-MFCs. This may be due to the accumulation of various cations that enter on the surface of clay by the specificity of the acrylic functional group which would improve the power in Out-C-MFCs. However, in the case of In-C-MFCs, it could have higher possibilities of an encounter with various cations (Na^+, K^+, Ca_2^+, $Mg_2^+$and NH_4^+) from the complex substrate (Rozendal et al., 2006) on the clay surface. Finally, the acrylic varnish could hinder the other cations and allow proton to complete the reaction. Meanwhile, saturation of various cations on the clay surface within a shorter period could cause less power (Derome and Lindroos, 1998). Without paint, C-MFCs show the least volumetric power production at the early stage and later start to decrease. This can be due to various factors, such as composition, thickness, and porosity. Which also might be responsible (Ajayi and Weigele, 2012; Winfield et al., 2013) for the limitation of proton transfer on clay, and for the lesser power production. It can be inferred that the acrylic-based varnish application on C-MFCs could greatly improve the performance of power production for a longer period.

EIS spectroscopy equivalent circuit obtained values in Table 1. The total internal resistance ($R_{int} = R_a + R_{s+e} + R_c$) of C-MFCs was distributed by the anodic and cathodic resistance (R_a and R_c), and Ohmic resistance of separator and electrolytes (R_{s+e}). Total R_{int} of C-MFCs follows the order: Both-C-MFCs (1307.63 Ohms) < In-C-MFCs (2881.54 Ohms) < Out-C-MFCs (4806.64 Ohms). Not-C-MFCs exhibited the higher internal resistance of 4975.14 Ohms. This discrepancy can be explained by the passage of ferricyanide solution that entered to the anodic chamber, which results in the loss of bacterial activity associated with the increase of anodic resistance and higher capacitance (Rahimnejad et al., 2015). However, this behavior in accordance with lower power production. While applying varnish on C-MFCs displays the reduction of R_{int}, especially Both-C-MFCs show the lesser R_{int}. Perhaps varnish coating on Clay cup separates the anodic and cathodic chamber and allows the specific transfer of ions by the action of fewer Rs + m.

Studies with the incorporation of a functional group on the neutral separator would facilitate specific counterions, reduce the internal resistance and improve the performance of microbial fuel cells (Sivasankaran et al., 2016; Kamaraj et al., 2015).

Table 1. Values obtained from the equivalent circuit obtained from the Nyquist plot of the electrochemical Impedance spectroscopy.

Resistance	Both-C-MFCs	Out-C-MFCs	In-C-MFCs	Not-C-MFCs
R_{s+m} (Ω)	5.00	6.00	7.00	9.00
R_{an} (Ω)	250.00	275.00	300.00	465.00
R_{cat}(Ω)	750.00	850.00	1100.00	4500.00

https://doi.org/10.1016/j.heliyon.2019.e01506

3.2. Closed circuit operation of C-MFCs

In a second bath operation, C-MFCs have carried out with the Closed-circuit of 3000 Ω for700 hrs, shown in Table 2. The average volumetric power densities was as follows: Both-C-MFCs (168.49 mW/m^3) >Out-C-MFCs (115.66 mW/m^3) >In-C-MFCs (61.54 mW/m^3) >Not-C-MFCs (27.21 mW/m^3). Both-C-MFCs shows the superior performance with gradually stable, which could mean that the acrylic-based varnish on both sides can improve the performance of C-MFCs with the longer operation. Doing a comparison between the results of Out-C-MFCs and In-C-MFCs, Out-C-MFCs reveals a higher performance. This agrees with the earlier statement. Without painting of acrylic varnish, it displays the least power production in the closed-circuit operation. Moreover, clay-based separator performance is limited by the thickness, composition, and porosity (Ajayi and Weigele, 2012; Winfield et al., 2013). In conclusion, the acrylic-based varnish can improve the performance of C-MFCs. In this experiment, a constant thickness of clay cup was maintained, further improved the performance by applying the acrylic-based varnish. The acrylic functional group has been reported already for their cationic exchange specificity (Kostov and Atanassov, 1993; Kariduraganavar et al., 1998).

The values obtained from the two cells of Both-C-MFCs connected in series and power the 4 digital clocks. It confirms the 91 % of COD removal and Avg. Power yield at 1.503 W/kg COD_R.

3.3. Physicochemical characterization of clay cub

Clay cup and acrylic varnish painted clay cup were analysed surface morphology and chemical composition by SEM images and EDAX, as presented in Fig. 3 a

Table 2. The average performance of the C-MFCs in closed-circuit operation (3k Ohm).

Parameters	Not-C-MFCs-3K	Both-C-MFCs-3K	In-C-MFCs-3K	Out-C-MFCs-3K
Avg. P_V (mW/m^3)	27.22	168.49	115.66	61.54
Avg. P (mW/m^2)	0.26	1.60	1.10	0.59
Avg. I_V (mA/m^3)	347.49	1011.69	798.25	455.41
Avg. I (mA/m^2)	3.30	9.61	7.58	4.33
Avg. Potential (V)	0.0273	0.110	0.086	0.049
Avg. Power yield (W/kg COD_R)	0.361	1.027	0.802	0.606
ηCOD (%)	64.69	85.05	80.71	77.45

Note. P_V (mW/m^3), volumetric power density; P (mW/m^2), anode area power density; I_V (mA/m^3), volumetric current density; I (mA/m^2), anode area current density; ηCOD (%), COD removal efficiency.

https://doi.org/10.1016/j.heliyon.2019.e01506

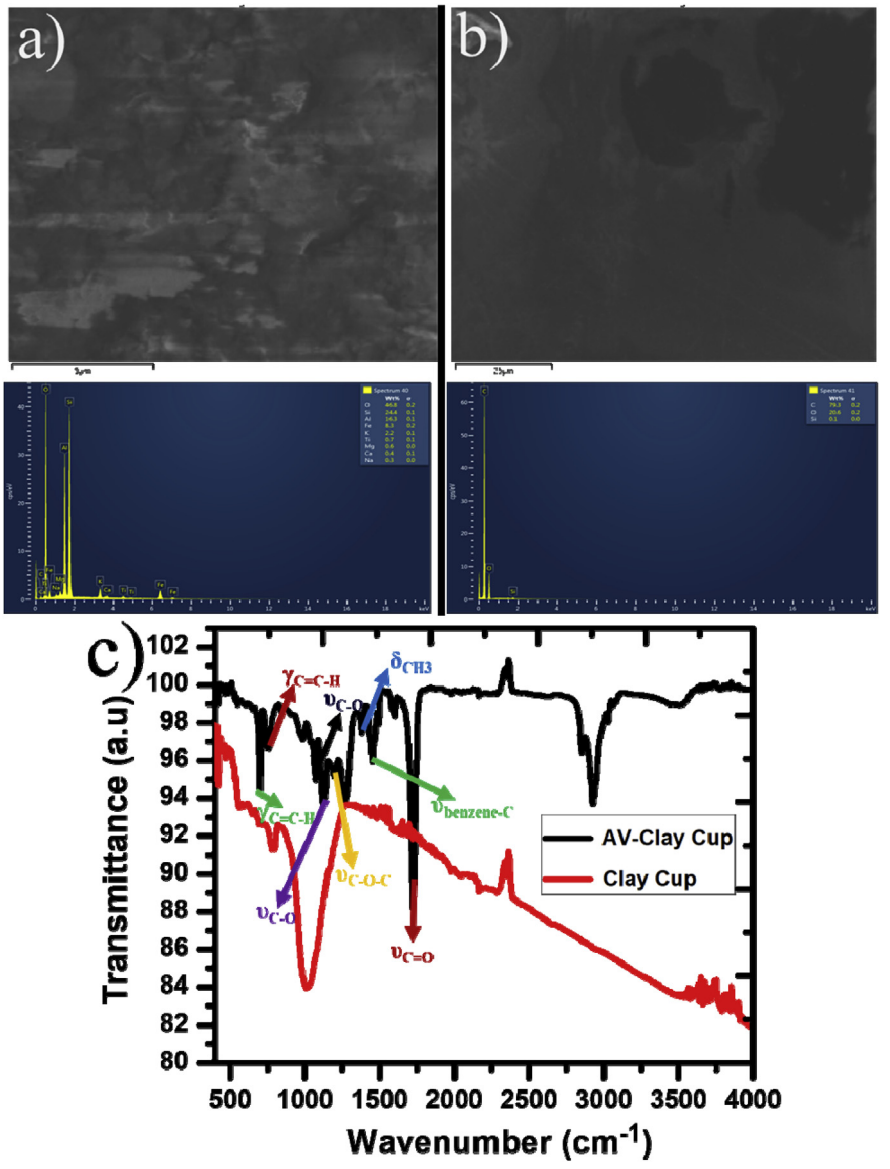

Fig. 3. Scanning electron microscopy and EDAX analysis of clay cup (a) and acrylic varnish painted clay cup surface (b). (C) Represent their FTIR analysis.

and b. clay cup surface exhibited the irregular pore size distribution and necessary chemical constitutions such as Si, Al, Fe, O, Ti, K, Mg, Ca and Na represent as clay. In the case of acrylic varnish, painted clay cup shows the regular distribution of acrylic varnish along the surface of the clay cup. After analysis of EDAX on the varnish, surface forms the defect at the corner of the image and revealed the major organic constitution on the surface (Fig. 3 b). The homogenized application of acrylic varnish on the clay cup along with the specificity of the acrylic group might improve the performance of acrylic varnish painted clay MFCs, which further justifies our previous arguments.

https://doi.org/10.1016/j.heliyon.2019.e01506

FTIR spectra of the clay cup and acrylic varnish painted clay are shown in Fig. 3 c. where the clay cup reveals the assigned to the stretching vibration bands of υ_{as} (−OH/inner hydroxyl) hydrogen bond with O-Si γ_{as} (inner hydroxyl) corresponding to 3696, 3619 and 3421 cm^{-1} δ(Si-O-Al) octahedral vibration exit at 1011 and 538 cm^{-1}. The additional band's exhibit at 701 and 755 cm-1 associated with surface hydroxyl. The OH^{-} Fe(II)Fe(III) OH absorbs peak near 800 cm^{-1} (Djomgoue and Njopwouo, 2013). Acrylic varnish painted clay cup reveals the fingerprint region that closer to the acrylic varnish. The bond vibration of $\upsilon_{C=O}$ and $\gamma_{C=C-H}$ represent at 1724 and 758 cm^{-1}. The peak of 1453 and 701 cm^{-1} corresponding to the $\upsilon_{benzene-C}$ and $\gamma_{C=C-H}$ vibration. δ_{CH3} bond exhibit at the 1382 cm^{-1}. The plane deformation vibration of υ_{C-O-C} found at 1236 cm^{-1}.1143 cm^{-1} shows the stretching bond of υ_{C-O}. The peak at 1067 cm^{-1} resulting from the υ_{C-O} bond stretching vibration (Chen et al., 2015).

3.4. Characterization of nopal biomass effluent

The initial parameters for the Nopal biomass effluent were the following: 3.45 g/l of COD, 7.4 of pH, 4.66 g/l of TDS, 9.32 mS/cm of conductivity (Fig. 4 a and b). During the operation of C-MFCs, both the Intermittent electrochemical characterization and the closed circuit performance with NBE substrate removal have enumerated the potential of MFCs to turn into wastewater treatment process along with power production. Both types of operation ensure the potential removal of the complex substrate as an electron donor and could influence the microflora composition. Moreover, we also accomplished the control experiment of NBE substrate removal under the flask condition (without included in C-MFCs). The highest COD removal of 85% was registered in a closed circuit operation of Both-C-MFCs, and the least COD removal was shown in Not-C-MFCs (64 %). Though, COD removal of

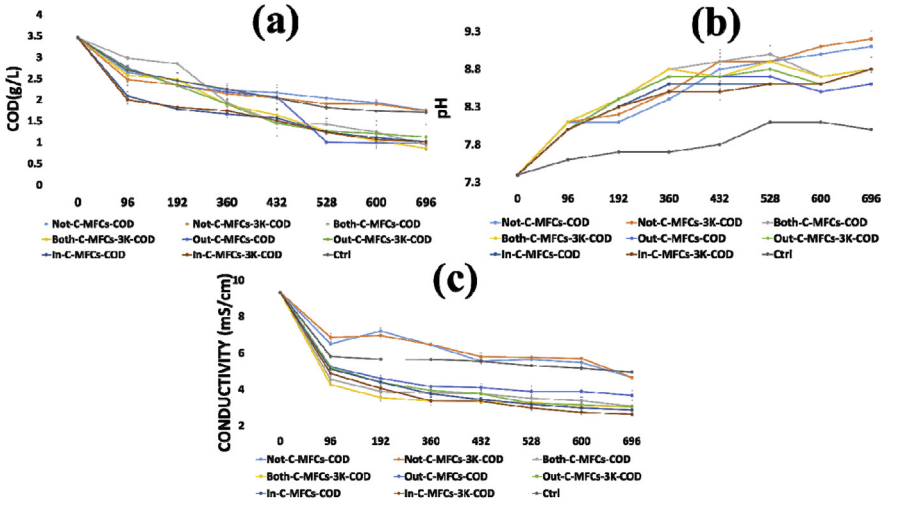

Fig. 4. COD (a), pH (b) and conductivity (c) of C-MFCs.

https://doi.org/10.1016/j.heliyon.2019.e01506

Both-C-MFCs of COD removal was observed at 72% and 53% for Not-C-MFCs under the intermittent electrochemical characterization. Interestingly, the closed circuit operation of C-MFCs (Both-C-MFCs, Out-C-MFCs, In-C-MFCs, and Not-C-MFCs) shows a COD removal superior to the intermittent electrochemical characterization. In conclusion, the oxidation of the substrate (NBE) by microbes was observed to be more effective/active at closed-circuit rather than at intermittent electrochemical characterization. This can be explained because the higher oxidation of NBE by the microbes is expected with a high ratio of oxidized electron carriers of the culture under the electrochemical stress over the microbes to remove the COD at a higher rate (Sathish-Kumar et al., 2012). Control experiment of NBE revealed 54 % of COD removal at the same period of C-MFC operation. Hence, the impose of MFCs technology on the complex biomass effluent/wastewater can be a promising resource to extract the electrical energy and reduce the cost of operation (Li et al., 2014).

Remarkably, control of NBE gradually increases towards alkaline pH (8.1). Moreover, under C-MFCs condition gradually reached the pH of 9.2. A slight increment of pH was observed on all the closed circuit operation than intermittent electrochemical characterization cells. This supports the argument that the electrochemical stress that imposes the bacteria to accelerate the oxidation rate of organic materials and results in alkaline pH might be associated with either carbonate or ammonia liberation on anolyte (Arogo et al., 2009).

Unexpectedly, the conductivity of the NBE and C-MFCs seeded with NBE(i.e. anolyte) gradually reduces. However, Not-C-MFCs of anolyte and NBE attained the 50% of conductivity losses (Fig. 4 c). Moreover, closed circuit operation and intermittent electrochemical characterization of anolyte In-C-MFCs, Out-C-MFCs, and Both-C-MFCs exhibited nearly 75% of Conductivity losses. The direct impact of this behavior was not well defined. Probably this behavior is being associated with the bioreduction of nitrate that promotes the demineralization of carbonate salt (Hamdan et al., 2011). At the final phase, based on the superior performance by Both-C-MFCs, two cells of Both-C-MFcs were connected in series in order to power to the digital clocks (Table 3 and Fig. 5) for 29 days. The average volumetric power density of 263.57 mW/m^3 at average Potential of 1.21 V with 91 % of COD removal was obtained during the operation. Unpredictably, the decline was observed at the 301 hrs. However, the performance again gradually increase and stable after that. This would ensure the potential application of MFCs in the complex substrate removal.

https://doi.org/10.1016/j.heliyon.2019.e01506

Table 3. Two cells of Both-C-MFCs connected in series to power the digital clocks operational parameters.

Parameter of Both-C-MFCs-CLK	
Avg. P_V (mW/m^3)	263.57
Avg. P (mW/m^2)	2.50
Avg. I_V (mA/m^3)	216.90
Avg. I (mA/m^2)	2.06
Avg. Potential (V)	1.21
ηCOD (%)	91.01
Avg. Power yield (W/kg COD_R)	1.503

3.5. Comparison of published work on clay-based dual chamber microbial fuel cells

A range of dual chamber clay based separator can be observed in Table 4. The main considerations of dual chamber microbial fuel cell design are the organic substrate, the cathodic electron acceptor and the type of ceramic materials used as membranes. The synthetic organic substrate has been used in most of the studies and can be responsible for higher power production (Jana et al., 2010). However, the economic viability of converting complex biogas effluent to power production is always

Fig. 5. Both-C-MFCs connected in series in order to power the digital clocks.

https://doi.org/10.1016/j.heliyon.2019.e01506

Table 4. Results from published work on separator type for microbial fuel cells.

Feed Stock	Ceramic type	Thick-ness (mm)	Struct-ure	Cathode Type	Max Power	Operation time	Prototype	Ref
Synthetic acetate	Earthen	4	Pot	KMnO4	70.48 W/m3	38 days	No	Behera et al. (2010a)
Rice mill wastewater	Earthen pot	4	Pot	Aerated	2.3 W/m3	288 h	No	Behera et al. (2010b)
Rice mill wastewater	Earthen pot	4	Pot	KMnO4	5.2 W/m3	288 h	No	Behera et al. (2010b)
Synthetic (sucrose)	Earthen	5	Cylinder	Permanganate	26.92 Wm3	26 days	No	Jana et al. (2010)
Synthetic (acetate)	Clayware	None given	Cylinder	NaClO	6.57 W/m3	20 days	No	Jadhav et al. (2014)
Synthetic (acetate)	Red soil	5	Pot	Aerated	1.49W/m3	22 days	No	Ghadge et al. (2014)
Synthetic (acetate)	Black soil	5	Pot	Aerated	1.12W/m3	22 days	No	Ghadge et al. (2014)
Biogas Effluent	Clay ware		Cylinder	Ferricyanide	1.8 W/m^3	432 hrs	Digital clocks (4)	This work

https://doi.org/10.1016/j.heliyon.2019.e01506

interesting and it depends on the integral composition of the bacterial community at the anode (Angenent and Wrenn, 2008; Chae et al., 2009).

The higher redox potential of Potassium permanganate and Sodium hypochlorite used as final terminal electron acceptors at cathode were revealed to attain the maximum power production (Behera et al., 2010a,b). Oxygen at the cathode is appreciable for environmental friendliness; however, it limits the power, due to large energy loss (Jadhav et al., 2014). The aforementioned studies demonstrated the success of implementing clay with different thickness based membrane used in dual chamber MFCs systems. Behera and Ghangrekar (2011) investigated the impact of clay thickness on power production, they realized that the clay with thinner walls exhibited lesser power production than the thicker walls. This can be directly explained by the longer path of protons or charged ion travel between two electrodes (i.e. anode and cathode). However, this effect is caused not because of the thickness alone, but also because of the composition/type of clay materials (Winfield et al., 2016). In the open literature, there is no report on the surface modification of clay. Clay cup modified with acrylic painted MFCs demonstrated a higher stability, extended to 432 h of operation with a higher concentration of biomass waste effluent served as an electron donor. Furthermore, the experiment demonstrates first to power the 4 digital clocks in connected two cells in a series exploring the use of the complex organic substrate (Fig. 5).

3.6. Abundance of bacterial phyla in the nopal biomass effluent seeded microbial fuel cells

High-throughput sequenced 16S rDNA libraries of control nopal biomass effluent (Ctrl NBE, i.e., in a sterile container) and nopal biomass effluent seeded Both-C-MFCs as Intermittent Electrochemical Characterized (Both-C-MFCs-IEC), and Closed Circuit Operation (Both-CMFC-3K) conditions, the suspended biomass (Both-C-MFCs-IEC and Both-CMFC-3K) and biofilms on the graphite felt (Both-C-MFCs-IEC-GF and Both-CMFC-3K-GF) were analysed for microbial community profiling as described in Materials and methods. From the analysis of initial control inoculum (Ctrl-NBE-Ini), 11 different bacterial phyla such as Acidobacteria, Actinobacteria, Bacteroidetes, Chloroflexi, Firmicutes, Synergistetes, Spirochaetes, TM7, SR1, Tenericutes, and Proteobacteria were identified. Among them, Firmicutes was the most abundant phylum; followed by Proteobacteria, Bacteroidetes, and Synergistetes in all fuel cells. In Both-C-MFC-3K-GF (10.6%) and Both-C-MFCs-IEC-GF (14.7%) cells showed a decrease in abundance of Synergistetes with respect to Control NBE-Ini (17.4%), and Control NBE-Fin (16.6%) (Fig. 6 a). The decreasing of microbial abundance could be related to the selection of the electrode respiration bacterial community under the electrochemical stress conditions provided. A similar

https://doi.org/10.1016/j.heliyon.2019.e01506

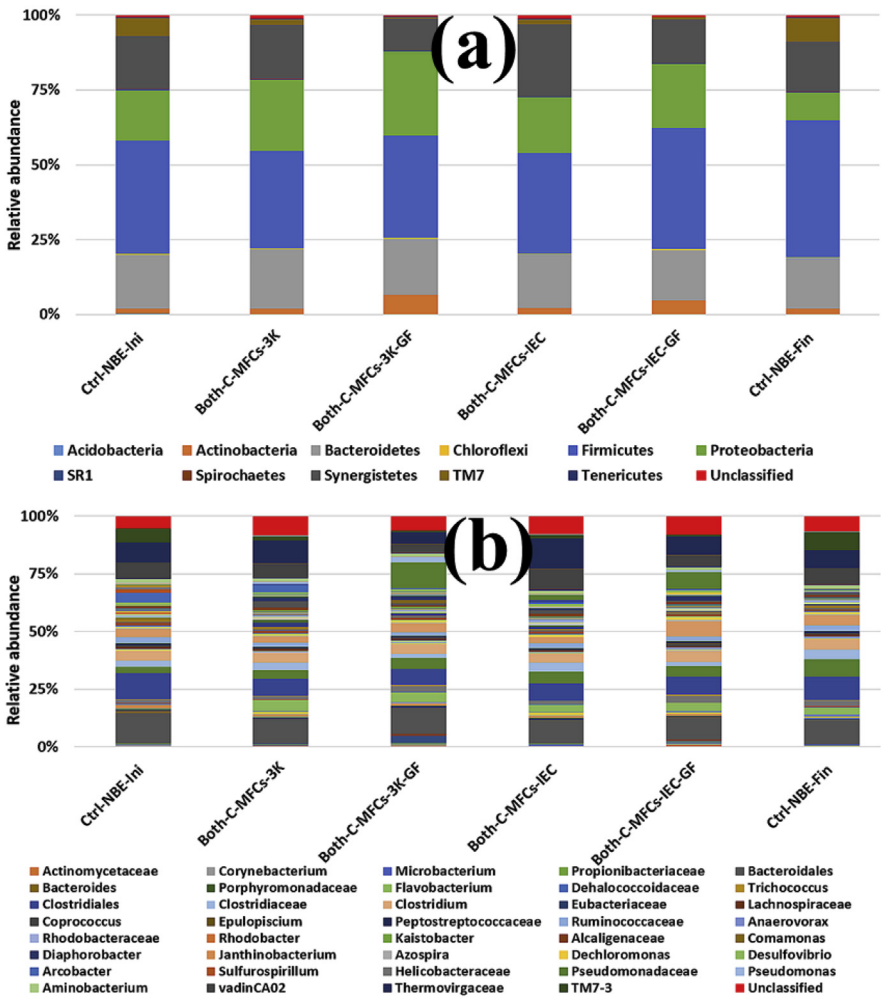

Fig. 6. Relative abundance of bacteria in C-MFCs. The figure shows a graphic display of the more abundant phyla and genera observed in the C-MFCs determined by high-throughput DNA sequencing of V3 16S rDNA libraries prepared from extracted genomic DNA from MFCs as described in Materials and methods. Y-axis shows % of relative abundance; X-axis indicates the abundance for a particular MFC; each taxonomic category is shown by a different color; a) phylum, b) genus.

type of decreasing abundance has been reported under substrate as a selection factor of electrode respiration bacteria (Baudler et al., 2014; Xiao et al., 2015).

On the other hand, the presence of Proteobacteria phyla abundance increased in all seeded MFCs. Proteobacteria relative abundance was 28.1% for Both-C-MFCs-3K-GF (both side varnish painted *cantarito* modified microbial fuel cell, 3K Ohm resistance fixed- Graphite felt)˃ 23.8% for Both-C-MFCs-3K ˃ 21.4% for Both-C-MFCs-IEC-GF> 18.5% for Both-C-MFCs-IEC. These abundances were larger than the 16.8% for Control NBE-Ini and the 9.4% for the Control NBE-Fin. Most of the previous reports on anodic communities were dominated by the presence of Proteobacteria phylum (Baudler et al., 2014; Xiao et al., 2015). Which further reveals that the

https://doi.org/10.1016/j.heliyon.2019.e01506

selection of anodic respiration bacterial communities is due to the electrochemical stressed condition used under closed circuit operation. The abundance of candidate phylum TM7 significantly decreased in seeded MFC in all conditions (Fig. 6 a). This candidate phylum was reported to be more abundant in soil and wastewater environments (Hanada et al., 2014). In general, an abundance of the rest of the bacterial phyla was almost unchanged during different stages of MFCs (Fig. 6 a).

3.7. Abundance of bacterial generating the nopal biomass effluent seeded microbial fuel cells

Sequenced data were also analyzed for the bacterial genus. In this case, the family Pseudomonadaceae increased from 0.24% in Control NBE-Ini, to 11.1% in Both-C-MFCs-3K-GF and to 7.4% in Both-C-MFCs-IEC-GF. It is worth to mention that the abundance of this family was only 0.18% in Control NBE-Fin at the end of the 696 h (Fig. 6 b). The Pseudomonadaceae family includes members of the *Azomonas* spp., *Azomonotrichon* spp., *Azorhizophilus* spp., *Azotobacter* spp., *Cellvibrio*

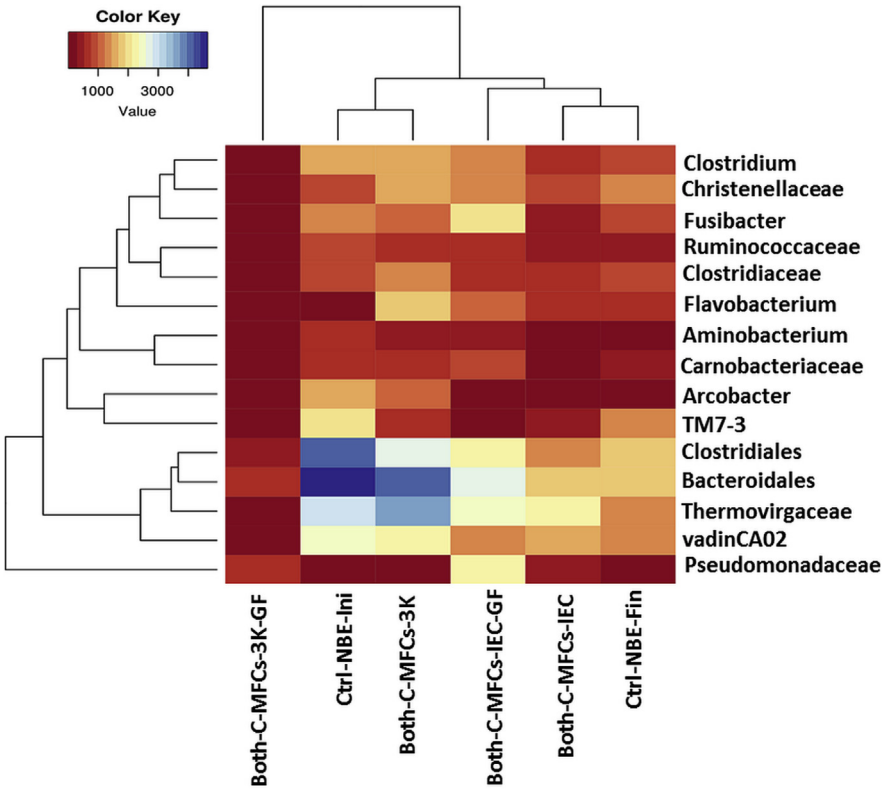

Fig. 7. Heatmap and hierarchical clustering of bacterial relative abundance C-MFCs. The figure shows in a color representation how different MFCs are clustered in the vertical axis and bacterial genera in the horizontal axis according to their abundance. The intensity of relative abundance ranges from 0-5000 OTUs; color intensity ranges from red (low abundance), white (medium abundance), to blue (high abundance).

https://doi.org/10.1016/j.heliyon.2019.e01506

spp., *Mesophilobacter* spp., *Pseudomonas* spp., *Rhizobacter* spp., *Rugamonas* spp., and *Serpens* spp. genera (Garrity, 2005).

A graphic heat map of the hierarchical clustering analysis at genus level of the top 15 genera (Fig. 7) shows that, in addition to members of the Pseudomonadaceae family, the Thermovirgaceae, Bacteroidales, Clostridiales, and Fusibacter were the most abundant families in the Both-C-MFCs-IEC-GF cell. We should mention that these bacteria were not as abundant in the Both-C-MFCs-3K-GF cell, or in the Control NBE-Ini and Control NBE-Fin controls.

Overall, there was no dysbiosis observed among MFCs. Although, when the change in particular bacteria abundance associated with the different C-MFCs was examined. It was found that five bacterial abundances were significantly more abundant in Control NBE-Ini/Fin than in Both-C-MFCs-3K/3K-GF and Both-C-MFCs-IEC/IEC-GF: Dehalococcoidaceae ($P = 0.043$), Clostridiales ($P = 0.010$) Lachnospiraceae ($P = 0.009$), Ruminococcaceae ($P = 0.017$), Anaerovorax ($P = 0.033$) and TM7-3 ($P = 0.016$). Further analysis revealed that Rhizobiales was significantly more abundant in Both-C-MFCs-IEC/IEC-GF ($P = 0.016$) and Bdellovibriowas significantly more in Both-C-MFCs-3K/3K-GF ($P = 0.005$) (Fig. 8).

3.8. Predicted functional profiling of nopal biomass effluent seeded microbial fuel cells

Microbial fuel cells functional metabolic pathway profile was predicted against the KEGG pathway, as mentioned in materials and methods. The relationship between the relative abundance of bacteria in the MFCs and KEGG metabolic pathways

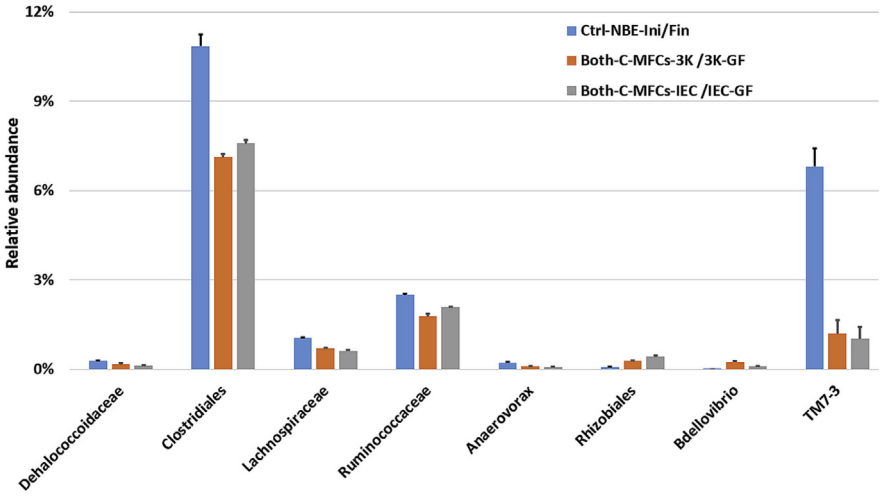

Fig. 8. Relative abundance of particular bacteria in C-MFCs. The histograms show the relative abundance of eight major bacterial genera found in Control, IEC and CCO-3K MFCs in this study. *$p < 0.05$, **$p < 0.01$. Y-axis, relative abundance of each bacteria; X-axis, Types of C-MFCs.

https://doi.org/10.1016/j.heliyon.2019.e01506

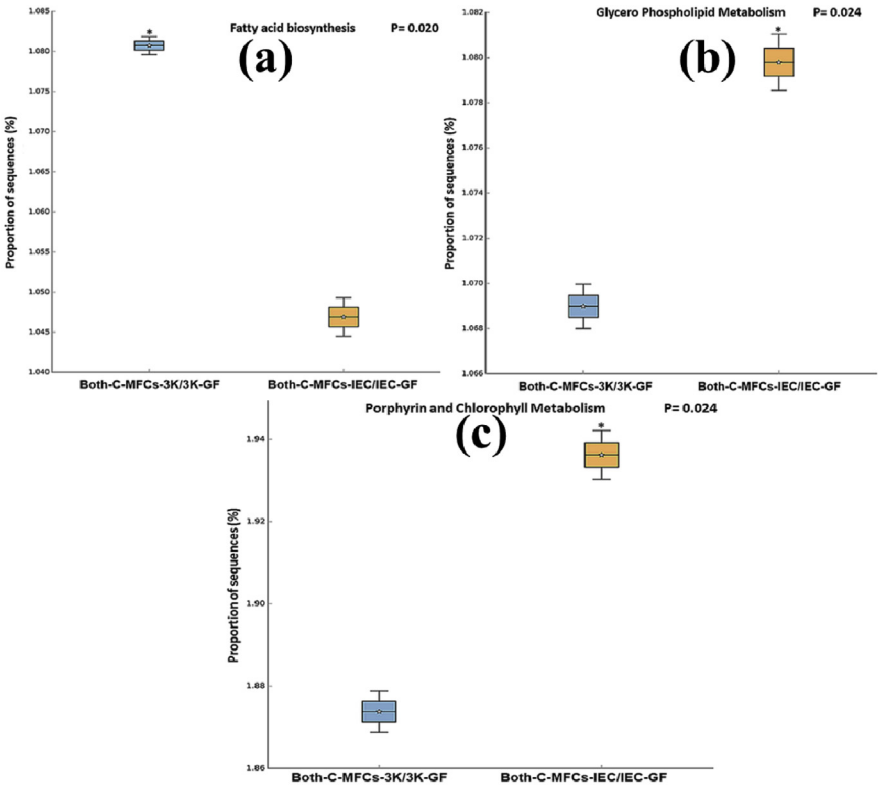

Fig. 9. Functional divergence between the Both-C-MFCs-3K/3K-GF than Both-C-MFCs-IEC/IEC-GF. (a) Genes in Fatty acid biosynthesis pathway (b) Glycero phospholipid metabolism c) Porphyrin and Chlorophyll metabolism pathways are significantly different between CCO-3K and IEC MFCs. *P $<$ 0.05,**P $<$ 0.01.

presented that Fatty acid biosynthesis (P = 0.020), Glycero Phospo lipid metabolism (P = 0.024) and Porphyrin and Chlorophyll metabolism (P = 0.024) were significantly different between Both-C-MFCs-3K/3K-GF and Both-C-MFCs-IEC/IEC-GF. Both-C-MFCs-IEC/IEC-GF showed significantly more Porphyrin and Chlorophyll metabolism than Both-C-MFCs-3K/3K-GF (Fig. 9). Porphyrins, a group of macrocyclic aromatic compounds, are capable to conduct effectively oxygen reduction reaction. When cobalt tetramethoxyphenylporphyrin as cocatalyst in MFC and maximum power output reached (Wang et al., 2011). Phospholipids serve as energy source upon hydrolysis and from lipid-based biofuels, the electrochemical energy produced upon electron transfer from substrate oxidation through wastewater microorganism as MFCs (Muller et al., 2014). The study predicted that Glycerol phospholipid functional profile was significantly higher in Both-C-MFCs-IEC/IEC-GF than Both-C-MFCs-3K/3K-GF. In a study based on fermented and hydrolyzed sludge, mixed volatile fatty acids were generated as a fuel source for MFCs (Freguia et al., 2010). Oxidation of NBE by microbes was more active at Both-C-MFCs-3K/3K-GF than Both-C-MFCs-IEC/IEC-GF and expected to liberate high ratio of

https://doi.org/10.1016/j.heliyon.2019.e01506

oxidized electron carriers of the NBE under the electrochemical stress (Sathish-Kumar et al., 2012). This explains the increase of fatty acid biosynthesis functional gene, which is due to oxidation inducing microbes in Both-C-MFCs-3K/3K-CF in this work to generate electricity.

4. Conclusion

C-MFCs modified with acrylic varnish improved the order for the maximum volumetric power densities were CCM-MFC:BS (1841.99 mW/m^3) > CCM-MFC:IS (1023.74 mW/m^3) > CCM-MFC:OS (448.90 mW/m^3). Further, the closed circuit operational power density was 205.03 mW/m^3 by the Both-C-MFCs. The control MFC without varnish exhibited poor performance, supporting the idea that acryloyl group would favor the cationic exchange results in higher stable power generation. Interestingly, the microbial analysis revealed that Rhizobiales was significantly more abundant in Both-C-MFCs-IEC/IEC-GF ($P = 0.016$) and Bdellovibriowas significantly more in Both-C-MFCs-3K/3K-GF ($P = 0.005$). The study predicted that Glycerol phospholipid functional profile was significantly higher in Both-C-MFCs-IEC/IEC-GF than Both-C-MFCs-3K/3K-GF.

Declarations

Author contribution statement

Sathish-Kumar Kamaraj: Conceived and designed the experiments; Analyzed and interpreted the data; Wrote the paper.

Alejandro Esqueda Rivera, Selvasankar Murugesan, Otoniel Maya: Performed the experiments; Wrote the paper.

Jaime García-Mena, Claudio Frausto-Reyes, José Tapia-Ramírez, Hector Silos Espino, Felipe Caballero-Briones: Analyzed and interpreted the data; Wrote the paper.

Funding statement

This work was supported by the CONACYT and Secretaría Educación Púbico (SEP)-Mexico, Cinvestav; CONACyT 163235 INFR-2011-01. Jaime García-Mena was supported by FONSEC SS/IMSS/ISSSTE-CONACYT-233361. Selvasankar Murugesan was supported by FONSEC SS/IMSS/ISSSTE-CONACYT-233361

https://doi.org/10.1016/j.heliyon.2019.e01506

Competing interest statement

The authors declare no conflict of interest.

Additional information

No additional information is available for this paper.

References

Ajayi, F.F., Weigele, P.R., 2012. A terracotta bio-battery. Bioresour. Technol. 116, 86–91.

Angenent, L.T., Wrenn, B.A., 2008. Optimizing mixed-culture bioprocessing to convert wastes into bioenergy. In: Wall, J.D., Harwood, C.S., Demain, A. (Eds.), Bioenergy. ASM Press, Herndon, VA, USA, pp. 179–194.

APHA, 1998. Standard Methods for the Examination of Water and Wastewater, twentieth ed. American Public Health Association/American water works Association/Water environment federation, Washington DC, USA.

Arogo, J., Wen, O., Ignosh, J., Bendfeldt, E., Collins, E.R., 2009. BiomethaneTechnology.College of Agriculture and Life Sciences. Virginia Polytechnic Institute and State University publication, pp. 442–881. https://www.pubs.ext.vt.edu/content/dam/pubs_ext_vt_edu/442/442-881/BSE-240.pdf.

Baudler, A., Riedl, S., Schröder, U., 2014. Long-term performance of primary and secondary electroactive biofilms using layered corrugated carbon electrodes. Front. Energy Res. 2 (30).

Behera, M., Ghangrekar, M.M., 2011. Electricity generation in low cost microbial fuel cell made up of earthenware of different thickness. Water Sci. Technol. 64 (12), 2468–2473.

Behera, M., Jana, P.S., Ghangrekar, M.M., 2010a. Performance evaluation of low cost microbial fuel cell fabricated using earthen pot with biotic and abiotic cathode. Bioresour. Technol. 101 (4), 1183–1189.

Behera, M., Partha, S., Jana, T., More, T., Ghangrekar, M.M., 2010b. Rice mill wastewater treatment in microbial fuel cells fabricated using proton exchange membrane and earthen pot at different ph. Bioelectrochemistry 79 (2), 228–233.

Borole, A.P., Hamilton, C.Y., Schell, D.J., 2013. Conversion of residual organics in corn stover-derived biorefinery stream to bioenergy via a microbial fuel cell. Environ. Sci.Technol. 47, 642–648.

https://doi.org/10.1016/j.heliyon.2019.e01506

Caporaso, J.G., Kuczynski, J., Stombaugh, J., Bittinger, K., Bushman, F.D., Costello, E.K., 2010. QIIME allows analysis of high-throughput community sequencing data. Nat. Methods 7 (5), 335–336.

Chae, K.J., Choi, M.-J., Lee, J.-W., Kim, K.-Y., Kim, I.S., 2009. Effect of different substrates on the performance, bacterial diversity, and bacterial viability in microbial fuel cells. Bioresour. Technol. 100, 3518–3525.

Chen, R., Lv, J., Feng, J., 2015. Characterization of paint by fourier-transform infrared spectroscopy, Raman microscopy, and scanning electron microscopy-energy dispersive X-ray spectroscopy. Anal. Lett. 48 (9), 1502–1510.

Cherubini, F., 2010. The biorefinery concept: using biomass instead of oil for producing energy and chemicals. Energy Convers. Manag. 51, 1412–1421.

Derome, J.R.M., Lindroos, A.J., 1998. Effects of heavy metal contamination on macronutrient availability and acidification parameters in forest soil in the vicinity of the Harjavalta Cu-Ni smelter, SW Finland. Environ. Pollut. 99, 225–232.

DeSantis, T.Z., Hugenholtz, P., Larsen, N., Rojas, M., Brodie, E.L., Keller, K., 2006. Greengenes, a chimera-checked 16S rRNA gene database and workbench compatible with ARB. Appl. Environ. Microbiol. 72 (7), 5069–5072.

Djomgoue, P., Njopwouo, D., 2013. FT-IR spectroscopy applied for surface clays characterization. J. Surf. Eng. Mater. Adv. Technol. 3 (4), 275–282.

Doyle, M., Rajendran, G., 2010. Perfluorinated Membranes in: Handbook of Fuel Cells, 3. John Wiley & Sons, Ltd. Fuel Cell Technol. Appl.

ElMekawy, A., Hegab, H.M., Dominguez-Benetton, X., Pant, D., 2013. Internal resistance of microfluidic microbial fuel cell: challenges and potential opportunities. Bioresour. Technol. 142, 672–682.

Freguia, S., The, E.H., Boon, N., Leung, K.M., Keller, J., Rabaey, K., 2010. Microbial fuel cells operating on mixed fatty acids. Bioresour. Technol. 101 (4), 1233–1238.

García-Mena, J., Murugesan, S., Pérez-Muñoz, A.A., García-Espitia, M., Maya, O., Jacinto-Montiel, M., 2016. Airborne bacterial diversity from the low atmosphere of greater Mexico city. Microb. Ecol. 72, 70–84.

Garrity, G., 2005. Bergey's manual of systematic bacteriology. In: Brenner, Don J., Krieg, Noel R., Staley, James R. (Eds.), The Proteobacteria Part B: the Gammaproteobacteria, Vol. 2. Williams & Wilkins.

Ghadge, A.N., Sreemannarayana, M., Duteanu, N., Ghangrekar, M.M., 2014. Influence of ceramic separator's characteristics on microbial fuel cell performance. J. Electrochem. Sci. Eng. 4 (4), 315–326.

https://doi.org/10.1016/j.heliyon.2019.e01506

Hamdan, N., Kavazanjian, E., Rittman, B.E., Karatas, I., 2011. Carbonate mineral precipitation for soil improvement through microbial denitrification. In: Han, J., Alzamora, D.A. (Eds.), Geo-frontiers : Advances in Geotechnical Engineering. American Society of Civil Engineers, Dallas.

Hanada, A., Kurogi, T., Giang, N.M., Yamada, T., Kamimoto, Y., Kiso, Y., Hiraishi, A., 2014. Bacteria of the candidate phylum TM7 are prevalent in acidophilic nitrifying sequencing-batch reactors. Microb. Environ. 29 (4), 353−362.

Hideo, K., Tsuzura, K., Shimizu, H., 1991. Ion Exchange Membranes, Ion Exchangers. Walter de Gruyter, Berlin.

Horan, J.L., Anitha, G., Hui, R., Benjamin, J.S., Mei-Chen, K., Fanqin, M., Steven, F.D., 2009. Copolymerization of divinylsilyl-11-silicotungstic acid with butyl acrylate and hexanediol diacrylate: synthesis of a highly proton-conductive membrane for fuel-cell applications. ChemSusChem 2 (3), 226−229.

Jadhav, D.A., Ghadge, A.N., Mondal, D., Ghangrekar, M.M., 2014. Comparison of oxygen and hypochlorite as cathodic electron acceptor in microbial fuel cells. Bioresour. Technol. 154, 330−335.

Jana, P.S., Behera, M., Ghangrekar, M.M., 2010. Performance comparison of upflow microbial fuel cells fabricated using proton exchange membrane and earthen cylinder. Int. J. Hydrogen Energy 35 (11), 5681−5686.

Kamaraj, S.-K., Romano, S.M., Moreno, V.C., Poggi-Varaldo, H.M., Solorza-Feria, O., 2015. Use of novel reinforced cation exchange membranes for microbial fuel cells. Electrochim. Acta 176, 555−566.

Kariduraganavar, F.M., Morneau, A., Mika, A.M., Childs, R.F., Roig, A., Molins, E., 1998. Polyacrylic acid pore-filled microporous membranes and their use in membrane-mediated synthesis of nanocrystallineferrihydrite. Can. J. Chem. 76, 10−17.

Karthikeyan, R., Sathishkumar, K., Murugesan, M., Berchmans, S., Yegnaraman, V., 2009. Bioelectrocatalysis of acetobacteraceti and gluconobacter-roseus for current generation. Environ. Sci. Technol. 43 (22), 8684−8689.

Kondaveeti, S., Kwang, S.C., Ramesh, K., Booki, M., 2014. Microalgae Scenedesmus obliquus as renewable biomass feedstock for electricity generation in microbial fuel cells (mfcs). Front. Environ. Sci. Eng. 8 (5), 784−791.

Kostov, G.K., Atanassov, A.N., 1993. Properties of cation-exchange membranes prepared by radiation graffing of acrylic acid onto tetrafluoroethylene − ethylene copolymer. J. Appl. Polym. Sci. 47, 1269.

https://doi.org/10.1016/j.heliyon.2019.e01506

Langille, M.G., Zaneveld, J., Caporaso, J.G., McDonald, D., Knights, D., Reyes, J.A., 2013. Predictive functional profiling of microbial communities using 16S rRNA marker gene sequences. Nat. Biotechnol. 31 (9), 814−821.

Li, W.-W., Yu, H.-Q., He, Z., 2014. Towards sustainable wastewater treatment by using microbial fuel cells-centered technologies. Energy Environ. Sci. 7 (3), 911−924.

Mason, P.M., Glover, K., Smith, J.A.C., Willis, K.J., Woods, J., Thompson, I.P., 2015. The potential of CAM crops as a globally significant bioenergy resource: moving from "fuel or food" to "fuel and more food. Energy Environ. Sci. 8, 2320−2329.

Min, B., Cheng, S., Logan, B., 2005. Electricity generation using membrane and salt bridge microbial fuel cells. Water Res. 39, 1675−1686.

Muller, E.E.L., Sheik, A.R., Wilmes, P., 2014. Lipid-based biofuel production from wastewater. Curr. Opin. Biotechnol. 30, 9−16.

Murugesan, S., Ulloa-Martínez, M., Martínez-Rojano, H., Galván-Rodríguez, F.M., Miranda-Brito, C., Romano, M.C., 2015. Study of the diversity and short-chain fatty acids production by the bacterial community in overweight and obese Mexican children. Eur. J. Clin. Microbiol. Infect. Dis. 34, 1337−1346.

Pant, D., Van Bogaert, G., Diels, L., Vanbroekhoven, K., 2010. A review of the substrates used in microbial fuel cells (MFCs) for sustainable energy production. Bioresour. Technol. 101 (6), 1533−1543.

Parks, D.H., Tyson, G.W., Hugenholtz, P., Beiko, R.G., 2014. STAMP: statistical analysis of taxonomic and functional profiles. Bioinformatics 30 (21), 3123−3124.

Rahimnejad, M., Ghasemi, M., Najafpour, G., Ismail, M., Mohammad, A., Ghoreyshi, A., Hassan, S.H., 2012. Synthesis, characterization and application studies of self-made Fe304/PES nanocomposite membranes in microbial fuel cell. Electrochim. Acta 85, 700−706.

Rahimnejad, M., Arash, A., Soheil, D., Alireza, Z., Sang-Eun, O., 2015. Microbial fuel cell as new technology for bioelectricity generation: a review. Alexandria Eng. J. 54 (3), 745−756.

Rozendal, R.A., Hamelers, Hubertus V.M., Buisman, Cees J.N., 2006. Effects of membrane cation transport on PH and microbial fuel cell performance. Environ. Sci. Technol. 40 (17), 5206−5211.

Sathish-Kumar, K., Omar, S.F., Gerardo, V.H., Luna-Arias, J.P., Héctor, M.P.-V., 2012. Electrical stress-directed evolution of biocatalysts community sampled from a

https://doi.org/10.1016/j.heliyon.2019.e01506

sodic-saline soil for microbial fuel cells. J. New Mater. Electrochem. Syst. 15, 181−186.

Sivasankaran, A., Dharmalingam, S., Young-Ho, A., 2016. Nanocomposite membranes based on sulfonated polystyrene ethylene butylene polystyrene (ssebs) and sulfonated Sio2 for microbial fuel cell application. Chem. Eng. J. 289, 442−451.

Ucar, D., Zhang, Y., Angelidaki, I., 2017. An overview of electron acceptors in microbial fuel cells. Front. Microbiol. 8, 643.

Wang, X., Cheng, S., Zhang, X., Li, X., Logan, B.E., 2011. Impact of salinity on cathode catalyst performance in microbial fuel cells (MFCs). Int. J. Hydrogen Energy 36, 13900−13906.

Winfield, J., Chambers, L.D., Rossiter, J., Ieropoulos, I., 2013. Comparing the short and long term stability of biodegradable, ceramic and cation exchange membranes in microbial fuel cells. Bioresour. Technol. 148, 480−486.

Winfield, J., Iwona, G., John, G., Ioannis, I., 2016. A review into the use of ceramics in microbial fuel cells. Bioresour. Technol. 215, 296−303.

Xiao, Y., Zheng, Y., Wu, S., Yang, Z.H., Zhao, F., 2015. Bacterial community structure of autotrophic denitrification biocathode by 454 pyrosequencing of the 16S rRNA Gene. Environ. Microbiol. 69, 492−499.

Zhang, Y., Olias, L.G., Kongjan, P., Angelidaki, I., 2011. Submersible microbial fuel cell for electricity production from sewage sludge. Water Sci. Technol. 64 (1), 50−55.

Zhao, N., Angelidaki, I., Zhang, Y., 2017. Electricity generation and microbial community in response to short-term changes in stack connection of self-stacked submersible microbial fuel cell powered by glycerol. Water Res. 109, 367−374.

Zhi, W., Ge, Z., He, Z., Zhang, H., 2014. Methods for understanding microbial community structures and functions in microbial fuel cells: a review. Bioresour. Technol. 171, 461−468.

https://doi.org/10.1016/j.heliyon.2019.e01506